Voltammetric and Scanning Electrochemical Microscopic Studies of the Adsorption Kinetics and Self-Assembly of *n*-Alkanethiol Monolayers on Gold

FARDAD FOROUZAN,[a] ALLEN J. BARD,[a,*] AND MICHAEL V. MIRKIN[b]
[a]Department of Chemistry and Biochemistry, The University of Texas at Austin, Austin, Texas 78712, USA
[b]Department of Chemistry and Biochemistry, Queens College-City University of New York, Flushing, New York 11367, USA

(Received 25 October 1996 and in revised form 27 May 1997)

Abstract. The adsorption kinetics and self-assembly of hexadecyl mercaptan on gold have been investigated by scanning electrochemical microscopy (SECM), chronoamperometry, and cyclic voltammetry. The developed methodology allows one to evaluate the surface coverage and the average size of the defects in the monolayer film from the effective rate constant of electron transfer. Two kinetic regimes of self-assembly were identified: a rapid initial adsorption of hexadecyl mercaptan onto a clean gold surface from 5 mM solution (more than 90% coverage obtained in 1 to 5 min), and a slower subsequent annealing of a thiol monolayer resulting in a more compact film. Typically, a long-chain-length thiol-treated gold surface acts as an electronically insulating surface after about 1 h. The SECM images of partially covered gold surfaces were always featureless, suggesting that the defects in the film were smaller than 0.5 μm for any exposure time ≥ 1 min.

INTRODUCTION

Self-assembly of molecular monolayers on surfaces has attracted considerable attention during the last several years as a means of surface modification as well as a model experimental system for studying long-distance electron transfer.[1,2] Slow adsorption of a long-chain (e.g., 16 C atoms) alkane thiol causes a gradual decrease in the electronically active surface of a gold electrode. The majority of self-assembled monolayer (SAM) studies to date have focused on investigating fully covered substrates.[3,4] Although the process of self-assembly can be monitored by different techniques, including scanning tunneling microscopy (STM), quartz-crystal microbalance studies, and voltammetry,[5–12] quantitative studies of adsorption kinetics and surface characterization of partially covered substrates remain scarce. Even high quality SAMs contain pinholes and other surface defects.[6] The defect density can be evaluated by scanning probe microscopies, e.g., STM, and atomic force microscopy; however, these imaging techniques do not always produce compatible results.[7] Specifically, AFM images do not show the random depressions (pits) seen in STM images. We report here information about the defect size and coverage from a combination of steady-state scanning electrochemical microscopic (SECM) measurements, chronoamperometry, and cyclic voltammetry. In these experiments, a dissolved redox species reacts to a Au electrode partially covered with long-chain thiol, and the dependence of the electrode response on the time of its exposure to a thiol solution is analyzed.

Interest in studying the adsorption kinetics, defect size, and density is twofold. First, when a SAM-coated electrode is used to probe electron transfer, a uniform, defect-free film is needed to obtain reliable kinetic data.[3,8] On the other hand, surfaces are sometimes intentionally modified with non-uniform monolayer films consisting of small patches with different chemical reactivities.[9] Such patterned surfaces have been proposed for sensor and catalysis applications. Passivating SAMs containing a controlled number of single-molecule "gate sites" were used to control the reactivity of an electrode.[10] The ability to control the kinetics of self-assembly, and knowledge of the size and density of active centers, are essential for such applications.

*Author to whom correspondence should be addressed. E-mail: ajbard@mail.utexas.edu.

In this study, thiol adsorption was monitored with the SECM, which can be employed to probe the surface reactivity of a uniform substrate as well as to distinguish locations of different reactivity on a surface and image reaction rate with submicrometer-scale resolution.[11] When the ultramicroelectrode (UME) tip is far from the substrate in a solution containing redox mediator, the tip current (i_T) quickly attains a steady-state value, $i_{T,\infty}$. When the tip is brought close (i.e., within a few tip radii) to a conductive substrate (Fig. 1) the regeneration of the redox mediator at the substrate produces an enhancement in the tip current ($i_T > i_{T,\infty}$). If the substrate is an electrical insulator or the redox kinetics at its surface are too slow, $i_T < i_{T,\infty}$ because of the hindered diffusion of redox species to the tip from the bulk solution. The smallest conductive island on the insulating surface observable with the SECM is of the order 0.1 a, where a is the tip radius.[11] Thus it should be possible to observe the individual defects of the SAM if they are well-separated and not smaller than 0.1 a (Fig. 1a). A surface covered with relatively large (defect radius, $R_d \geq 0.1\ a$) and poorly separated conductive features will appear uniformly conductive because the individual diffusion fields overlap (Fig. 1b). No individual defects can be observed by the SECM in this case. Small and sparse defects on the insulating surface do not produce any detectable feedback current, and such a surface appears to be uniformly insulating (Fig. 1c). Finally, a surface with small ($R_d \leq 0.1\ a$), closely spaced defects will appear partially conductive, with the average reactivity depending on the size and density of the conductive spots (Fig. 1d). The SECM response in this case should mimic the effect of finite heterogeneous kinetics at the substrate.

THEORY

A theory for both steady-state and time-dependent processes at a partially covered electrode with microscopic active zones is needed to interpret our experimental results. We assume that the SAM defects possess a disc shape rather than a strip shape. Note that as the SAM becomes more compact and the defects get smaller, the local current density increases greatly and the overall redox process may become kinetically-controlled.

Application of the Zwanzig–Szabo Treatment to the Analysis of the Steady-State SECM Response and Potentiostatic Transients

Different approaches have been proposed to treat the diffusion kinetics at a partially covered electrode and for an array of inlaid microdisc electrodes.[12–15] Among these, the treatments of Zwanzig and Szabo[13,14] and Amatore et al.[15] are most closely related to our experimental system. The theory developed in ref 15 should be applicable to any transient and steady-state experiment with a regular array of microscopic discs (i.e., with a constant center-to-center distance). The derivation, based on the effective medium approximation,[13,14] yielded two expressions for the steady-state diffusion current to an inert sphere partially covered by randomly distributed active discs (with the overall process controlled either by diffusion or finite heterogeneous kinetics), and for a diffusion-controlled chronoamperometric curve (potential step) at such an array. Transients obtained at regular and random arrays of microdiscs are significantly different.

The steady-state diffusion-limited current to an insulating sphere of radius R_{sp} partially covered by N identical electroactive discs can be expressed as[13]

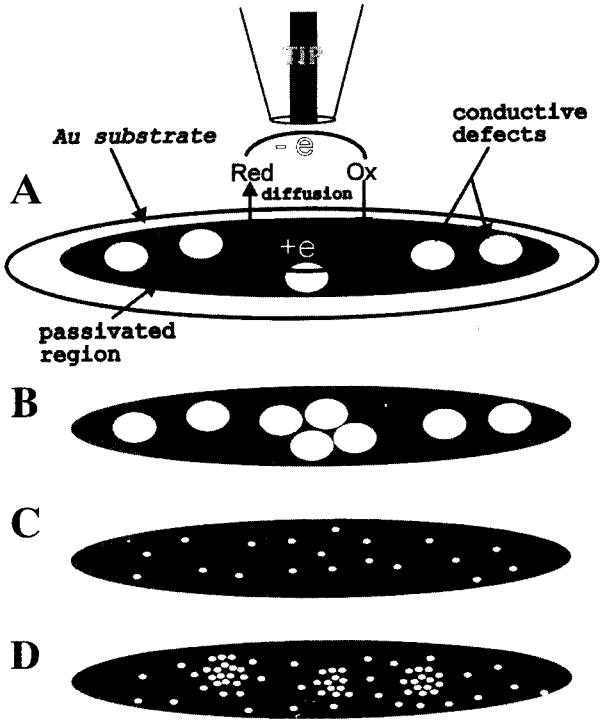

Fig. 1. Schematic diagram of the SECM experiment with a gold substrate partially covered with a long-chain thiol layer. The monolayer defects are assumed to be disc-shaped. The rate of mediator regeneration at the SAM-passivated surface is negligible. The tip current is a function of the surface coverage θ and average defect radius R_d. (A) Individual defects can be imaged only when they are well separated and R_d is comparable with the tip radius. (B) Defects are large but not well separated and thus cannot be observed individually. (C) Defects are small and sparse, and the substrate behaves as an insulator. (D) Small ($R_d < 0.1\ a$) closely spaced defects produce the averaged response mimicking slow heterogeneous kinetics at the substrate.

$$i_d = \frac{N i_{sphere} i_{disc}}{\theta i_{sphere} + N i_{disc}} \quad (1)$$

where

$$i_{sphere} = 4\pi nFDR_{sp}c^\circ \quad (2a)$$

and

$$i_{disc} = 4nFDR_d c^\circ \quad (2b)$$

are steady-state diffusion currents to a disc and an electroactive sphere. R_d is the disc radius, D is the diffusion coefficient, c° is the bulk concentration of the electroactive species, F is the Faraday constant, n is the number of electrons transferred per redox event, and

$$\theta = 1 - NR_d^2/4R_{sp}^2 \quad (3)$$

is the fraction of surface that is insulating, i.e., free from electroactive disc-shaped defects. The diffusion current values computed from eq 1 were in agreement with the results obtained by digital simulation.[13b] For $\theta \rightarrow 1$, eq 1 can be rewritten as

$$\frac{1}{i_d} = \frac{1}{i_{sphere}} + \frac{1}{N i_{disc}} \quad (4)$$

Equation 2 can be compared to the equation for a steady-state current i_{kin}^{un} due to the irreversible heterogeneous reaction at a uniformly reactive sphere of the same radius:

$$\frac{1}{i_{kin}^{un}} = \frac{1}{i_{sphere}} + \frac{1}{4\pi R_{sp}^2 nFc^\circ k_{eff}} \quad (5)$$

where k_{eff} is the heterogeneous rate constant for a uniform sphere. When the second terms in the right hand side of eqs 4 and 5 are equal, the quantities in the left hand sides of both equations become equal too. Thus the diffusion-controlled steady-state current to a partially covered sphere mimics the kinetically-controlled current to a uniform sphere of the same radius with a $k_{eff} = Ni_{disc}/4\pi R_{sp}^2 nFc^\circ = NDR_d/\pi R_{sp}^2$. From eq 3, this effective rate constant is proportional to the fraction of the surface area covered by conductive discs $(1 - \theta)$

$$k_{eff} = 4(1 - \theta)D/\pi R_d \quad (6)$$

When the process at the microdiscs is governed by finite irreversible heterogeneous kinetics (i.e., the diffusion flux to the disc is $J = kc$, where k is the heterogeneous rate constant, and c is the local concentration of electroactive species at the disc surface), and $\theta \rightarrow 1$, the expression for the total steady-state current to the sphere can be derived from eqs 13, 15, and 17 in ref 13b:

$$\frac{1}{i_{kin}} = \frac{1}{i_{sphere}} + \frac{1}{N i_{kin}^{disc}} \quad (7)$$

where i_{kin}^{disc} is a steady-state current to an individual disc of a radius R_d due to the irreversible heterogeneous reaction with a rate constant κ. i_{kin}^{disc} can be expressed either as[16]

$$i_{kin}^{disc} = \frac{i_{disc}}{1 + \frac{\pi}{\kappa}\frac{2\kappa + 3\pi}{4\kappa + 3\pi^2}} \quad (8)$$

or as (see eq B26 in ref 13b)

$$i_{kin}^{disc} = \frac{15 + 64/\kappa}{15 + 84/\kappa + 64/\kappa^2} i_{disc} \quad (9)$$

where $\kappa = \pi k R_d/4D$. The values computed from eqs 8 and 9 agree to within 1% for $0.1 \le \kappa \le 10$. From eqs 5, 7, and 8, one concludes that the steady-state response of a partially covered spherical electrode under finite kinetic control (i.e., with a heterogeneous constant k for all reactive discs and surface coverage $1 - \theta$) should be equivalent to the kinetically controlled current to the uniform sphere of the same radius and

$$k_{eff} = \frac{4(1 - \theta)D}{\pi R_d\left[1 + \frac{\pi}{\kappa}\frac{2\kappa + 3\pi}{4\kappa + 3\pi^2}\right]} \quad (10)$$

It is not possible to distinguish between the diffusion-controlled process at the disc-shaped defects (eqs 5 and 6) and finite heterogeneous kinetics (eqs 7–10) in a single current measurement. However, by shifting the electrode potential to more extreme values, the diffusion limit where the effective rate constant (k_{eff}) becomes potential-independent can be reached.

Note that a sphere is just an example of a uniformly accessible electrode. Not only steady-state but also time-dependent equations for a partially covered sphere can be generalized for any electrode whose surface is uniformly accessible.[14] Thus eqs 6 and 10 should hold true for any nearly completely covered by insulator ($\theta \rightarrow 1$) uniformly accessible electrode at steady-state. In particular, SECM current–distance (i_T–d) curves obtained with a partially covered substrate should have the same shape as the kinetically controlled i_T–d curve at an uncovered substrate. The latter can be described by the following equation:[17]

$$I_T^\kappa = \left[\frac{0.78377}{L(1 + 1/\Lambda)} + \frac{0.68 + 0.3315\exp(-1.0672/L)}{1 + F(L,\Lambda)}\right]\times \quad (11)$$

$$(1 - I_T^{ins}/I_T^c) + I_T^{ins}$$

where I_T^c, I_T^K, I_T^{ins} represent the tip current for the diffusion-controlled regeneration of a redox mediator, finite substrate kinetics, and insulating substrate (i.e., no mediator regeneration), respectively, at a normalized tip–substrate separation, $L = d/a$. k_{eff} is the apparent heterogeneous rate constant (cm/s), $\Lambda = k_{eff}d/D$, D is the diffusion coefficient of a redox mediator, and $F(L,\Lambda) = (11 + 7.3\Lambda)/\Lambda/(110 - 40L)$. All I_T^c, I_T^K, and I_T^{ins} are normalized by the tip current at an infinite tip–substrate separation, $i_{T,\infty} = 4nFaD_{Red}c^\circ$. The analytical approximations for I_T^c and I_T^{ins} are[18]

$$I_T^c = 0.78377/L + 0.3315\exp(-1.0672/L) + 0.68 \quad (12)$$

$$I_T^{ins} = 1/(0.15 + 1.5358/L + 0.58\exp(-1.14/L) + 0.0908\exp[(L-6.3)/(1.017L)] \quad (13)$$

Szabo and Zwanzig[13,14] also obtained an equation describing a diffusion-controlled chronoamperogram at a partially covered electrode ($\theta > 0.5$) that can be rewritten using our notation as

$$i(t) = (1-\theta)i_{cott}(t) + \frac{nFc^\circ DA(1-\theta)\theta}{R_d} \times \left[\frac{\lambda_+ - 4\alpha/\pi}{\lambda_+ - \lambda_-}\exp(\lambda_+^2 Dt/R_d^2)\,\mathrm{erfc}\left(\sqrt{\lambda_+^2 Dt/R_d^2}\right) + \frac{4\alpha/\pi - \lambda_-}{\lambda_+ - \lambda_-}\exp(\lambda_-^2 Dt/R_d^2)\,\mathrm{erfc}\left(\sqrt{\lambda_-^2 Dt/R_d^2}\right)\right] \quad (14)$$

where $i_{cott}(t) = nFc^\circ A\sqrt{D/\pi t}$ is the Cottrell current to the unblocked electrode of the same surface area A, $\alpha = \pi(4-\pi)/(\pi^2-8) \cong 1.4424$, and $\lambda_\pm = 0.5(1 - \theta + \alpha \pm [(1-\theta+\alpha)^2 - 16(1-\theta)\alpha/\pi]^{1/2})$. The R_d and θ values can be found by fitting experimental chronoamperograms to eq 14.

Treatment of Amatore et al.[15]

Unlike the approach of Szabo and Zwanzig, which is solely applicable to chronoamperograms, and more precise, the model developed by Amatore et al. is applicable to the analysis of both non-steady-state CVs and CAs at a partially blocked electrode with microscopic defects ($\theta \to 1$), and is more approximate. The derivation of the main equations in ref 15 relies on a number of approximations, and for some of them no adequate error analysis was reported. Moreover, the accuracy was discussed in terms of surface concentrations, though in some cases (e.g., a quasi-reversible voltammogram at potentials near E°) a 1% error in calculation of the surface concentration may result in wrong current values by orders of magnitude. Although it is hard to check the validity of the equations[15] in general, for a diffusion-controlled steady-state process, a comparison with eq 1 is straightforward. The derivation in ref 15 follows the logic of the earlier work by Smythe[19] to establish the equivalence between the partially blocked surface and a uniform surface of the same area and finite reactivity. The dimensionless parameters introduced in ref 15 are most suitable for non-steady-state voltammetry. For steady-state conditions, the main approximation for disc-type defects (eq 9 in ref 15) can be rewritten as

$$c_0 = c_\mu - 2R_0JF(1-\theta) \quad (15)$$

where $R_0 = R_d/(1-\theta)^{1/2}$, c_0 is the average surface concentration of the electroactive species at a disc-shaped defect on a partially covered surface and c_μ and J are the surface concentration and its normal derivative for the equivalent uniformly accessible surface; $J = (\partial c/\partial n)_\mu = (1-\theta)(\partial c/\partial n)_0$. When the process at a partially covered surface is diffusion limited, i.e., $c_0 = 0$, $F(1-\theta) = (\pi/8)(1-\theta)^{-1/2}$ (see eq 8a in ref 15) and

$$c_\mu = \pi R_0 J(1-\theta)^{-1/2}/4 = \pi R_d J/4(1-\theta) \quad (16)$$

If the surface of interest is a large sphere partially covered with conductive discs and $R_{sp} >> R_d$, the steady-state current can be expressed as

$$i = 4\pi nFR_{sp}D(c^\circ - c_\mu) = 4\pi nFR_{sp}D \times [c^\circ - \pi R_d J/4(1-\theta)] = 4\pi R_{sp}^2 nFDJ \quad (17)$$

Thus

$$J = \frac{c^\circ}{R_{sp} + \pi R_d/4(1-\theta)} \quad (18)$$

The combination of eqs 18, 1, 2, and 3 gives

$$i = \frac{4\pi R_{sp}^2 nFDc^\circ}{R_{sp} + \pi R_{sp}^2/NR_d} = \frac{4\pi NnFR_{sp}R_dDc^\circ}{NR_d + \pi R_{sp}} = \frac{i_{sphere}NR_d}{NR_d + \pi R_{sp}} = \frac{Ni_{sphere}i_{disc}}{Ni_{disc} + i_{sphere}} \quad (19)$$

This result is identical with the Berg–Purcell formula.[20] It becomes equivalent to eq 1, which represents a corrected Berg–Purcell formula,[13] as $\theta \to 1$.

One cannot, however, expect the non-steady-state chronoamperograms obtained according to ref 15 to be in a quantitative agreement with eq 14. Amatore's model assumes a constant center-to-center distance and thus is expected to yield somewhat higher current values. The same qualification should apply to cyclic

voltammograms; however, the theory developed in ref 15 should be suitable for semi-quantitative analysis of our experimental data.

EXPERIMENTAL SECTION

Chemicals

Hexadecyl mercaptan, ammonium hexafluorophosphate 99.99% (Aldrich Chemical Co., Milwaukee, WI), and ferrocenylmethyltrimethylammonium iodide (Strem Chemicals, Newburyport, MA) were used as received. Ferrocenylmethyltrimethylammonium hexafluorophosphate, $FcTMAPF_6$, was synthesized from the addition of a saturated solution of NH_4PF_6 to a solution of TMAFcI dissolved in water. $FcTMAPF_6$ precipitated out of solution and was washed with cold water and dried under vacuum. All aqueous solutions were prepared from deionized water (Milli-Q, Millipore Corp.).

Electrodes and Electrochemical Cells

7-μm-diameter carbon fibers (Union Carbide Co.) were heat-sealed in Pyrex tubes under vacuum and then beveled to produce SECM tips, as described previously.[21] These electrodes were polished with 0.05-μm alumina before each set of experiments and were used as the working electrode in a three-electrode electrochemical setup. The counter electrode was a 1-mm-diameter Pt wire that was immersed into the electrolyte about 1.5 cm. The reference electrode was Ag/AgCl (3 M KCl). The SECM electrochemical cell was constructed from Teflon and covered with a circular glass top to keep the cell free of oxygen. This glass top had small openings which allowed for easy electrolyte access and a larger hole through which the SECM tip could approach the substrate. The electrolyte was purged with N_2 through the small openings prior to each experiment. The cell design allowed for the easy polishing of a removable bottom section which had a 1-mm-diameter Au wire substrate sealed into it. The total electrolyte volume used in the SECM experiments was about 3.5 cm^3.

SECM Apparatus and Procedure

The SECM apparatus has been discussed previously.[22] The movement of the SECM tip was controlled by three piezoelectric inchworm motors controlled by a CE-1000 micropositioning device (Burleigh Instruments, Fishers, NY). The SECM setup, including the electrochemical cell, was mounted on a vibration-free stage. An EI-400 bipotentiostat (Ensman Instrument, Bloomington, IN) was used for potential control and current measurement. The approach curves were obtained by recording the SECM tip current, $i_{T,\infty}$, as a function of the tip distance from the substrate, d. The bipotentiostat was interfaced to a personal computer through an analog/digital converter.

Thiol Treatment

Prior to each set of experiments, the substrate was polished with 0.05-μm alumina and sonicated for 15 min to remove any alumina particles that may have been embedded onto the Au surface during the polishing procedure. A 5 mM hexadecyl mercaptan solution in EtOH was used to cover the Au substrate for the desired time period. The treated Au surface was rinsed off with an excess of EtOH for 30 s followed by rinsing with distilled deionized water for 1 min. After each experiment, the substrate was rinsed with distilled deionized water for 1 min and EtOH for 30 s prior to re-exposure to the thiol solution for longer time periods. The exposure times given are the total integrated times, e.g., the electrode was exposed for 1 min, a measurement was made, and the electrode was then returned to the thiol solution for an additional 4 min (total exposure time, 5 min).

RESULTS AND DISCUSSION

SECM Imaging

To obtain qualitative information about the size and distribution of defects in SAMs we used the SECM with a 7-μm-diameter C tip to image the thiol-covered Au substrate. The tip current (at the same tip–substrate distance) decreased with an increase in exposure time (from 1 min to hours) of the Au to the thiol solution. SECM images of an Au substrate were obtained in a 2 mM aqueous solution of $FcTMAPF_6$ in 0.2 M LiCl with the tip biased at +0.45 vs. Ag/AgCl. The substrate was kept unbiased and was at a potential about 250 mV negative of the $FcTMAPF_6$ reduction potential. We therefore assume that ferrocenium reduction at the substrate was diffusion-controlled. Equation 11 was used to convert the SECM feedback currents to distance values. Figure 2a shows the substrate surface marked by touching a 10-μm-diameter disc-shaped tip to the surface after it was polished with 0.05-μm alumina. Figure 2b shows the same surface after a 15-min exposure to the thiol solution. These marks cannot be seen in Fig. 2b because the resolution of constant potential SECM imaging is lower for insulators than for conductors. A comparison of Figs. 2a and b does not show any new topographic features attributable to islands of thiol or defects in the monolayer. With a 7-μm-diameter tip, the radius of the smallest detectable conductive feature would be slightly less than 0.5 μm.[11] The homogeneous featureless images obtained in all SECM experiments suggest that the defects or islands for all exposure times in our experiments (i.e., $t_e \geq 1$ min) were smaller than 0.5 μm. The main difference between the two images is that the substrate appears conductive ($i_T > i_{T,\infty}$) before, and insulating ($i_T < i_{T,\infty}$) after, it was exposed to thiol. Amatore et al.[15] showed that for such systems their formalism is more appropriate than that developed by Matsuda et al.,[23] and this model can be used in the voltammetric experiments.

Cyclic Voltammetry

A series of cyclic voltammograms of $FcTMAPF_6$ obtained at a 1-mm-diameter gold electrode is presented

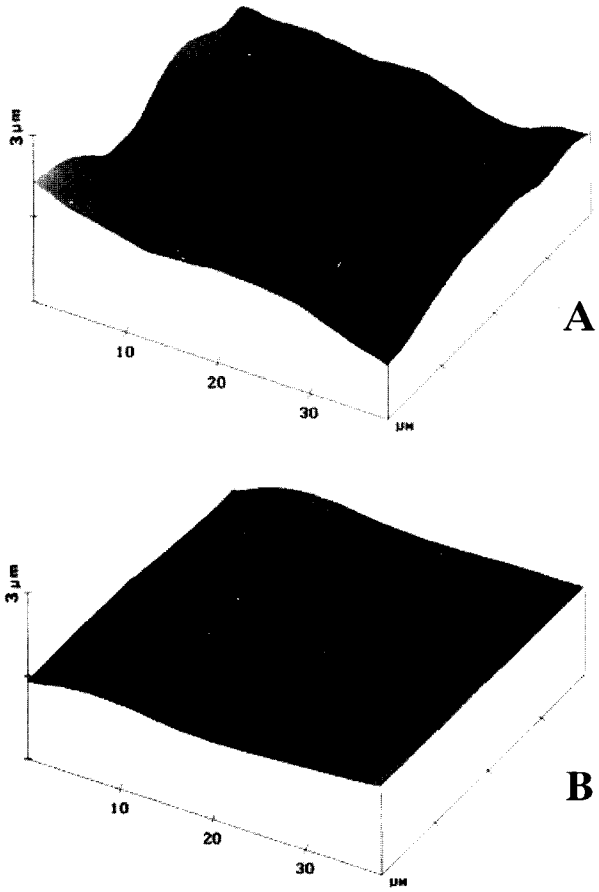

Fig. 2. Constant height SECM image of the gold substrate before (A) and after (B) 15 min of exposure to a 5×10^{-3} M solution of hexadecyl mercaptan. The tip was a 3.5-μm-radius carbon fiber biased at +0.45 vs. Ag/AgCl (3 M KCl). The aqueous solution contained 2×10^{-3} M $FcTMAPF_6$ and 0.2 M LiCl. $i_{T,\infty} = 1.2 \times 10^{-9}$ A. Eq 11 was used to convert the SECM feedback currents to distance values.

in Fig. 3. The curves in this figure were obtained by varying the exposure time of the gold surface to thiol solution from $t_e = 0$ min (curve 1) to $t_e = 50$ min (curve 7). Clearly, both anodic and cathodic peak currents decrease with increasing exposure time, and after $t_e = 50$ min, the surface becomes essentially passivated. Curve 7 is very similar to the voltammogram obtained with only the supporting electrolyte present in solution. This shows that the hydrocarbon chain of hexadecyl mercaptan is sufficiently long to make the electron-transfer rate negligible under our experimental conditions.

According to ref 15, the shape of the cyclic voltammograms obtained at a partially blocked electrode is determined by two dimensionless parameters:

$$K\lambda^{1/2} = 1.67 \sqrt{\frac{DRT}{Fv}} \frac{1-\theta}{R_d} \qquad (20)$$

and

$$\Lambda(1-\theta) = \sqrt{\frac{RT}{FvD}}\, k^\circ(1-\theta) \qquad (21)$$

where k° is the standard heterogeneous rate constant at the reactive discs and v is the potential sweep rate. Four possible types of CVs were presented in a zone diagram[15] corresponding to the extreme values of these parameters: Zone 1, nernstian cyclic voltammogram, $\Lambda(1-\theta) >> 1$ and $K\lambda^{1/2} >> 1$; with respect to Fig. 3, where $D = 5 \times 10^{-6}$ cm²/s, $v = 0.01$ V/s, and $k^\circ \approx 1$ cm/s, this limiting case corresponds to $1-\theta >> 0.001$ and $(1-\theta)/R_d >> 200$. Zone 2, irreversible cyclic voltammogram, $\Lambda(1-\theta) << 1$ and $K\lambda^{1/2} >> 1$; i.e., $1-\theta << 0.001$ and $(1-\theta)/R_d >> 200$. From the latter two inequalities $\theta > 0.999$ and $R_d << 10^{-5}$ cm. Zone 3, irreversible steady-state voltammogram, $\Lambda(1-\theta) << 1$ and $K\lambda^{1/2} << 1$; i.e., $1-\theta << 0.001$ and $(1-\theta)/R_d << 200$. Zone 4, nernstian steady-state voltammogram, $\Lambda(1-\theta) >> 1$ and $K\lambda^{1/2} << 1$; i.e., $1-\theta >> 0.001$ and $(1-\theta)/R_d << 200$. This means that $\theta < 0.999$ and $R_d >> 10^{-5}$ cm.

The first zone corresponds to a nernstian cyclic voltammogram with a peak separation of about 60 mV. Curves 1 (uncoated gold), 2, and 3 (1 and 5 min exposures to thiol, respectively) in Fig. 3 belong to this category. At longer exposure times, the peak separation increases. Curves 4 and 5 fall into the transition region between zone 1 and zone 2 and $0.99 < \theta < 0.9999$ for these curves (Fig. 3 in ref 24). Accordingly, the upper limit for R_d decreases to about 5 nm. Finally, at $t_e \approx 40$ min, the reverse (cathodic) peak disappears, and the shape of the voltammogram tends to become sigmoidal, with the half-wave potential significantly more positive than the formal potential of $FcTMAPF_6$ (curve 6). This corresponds to the transition from zone 2 to 3, which is consistent with a further increase in θ, which clearly approaches unity at $t_e \geq 50$ min (curve 7 in Fig. 3).

The above semiquantitative analysis shows that almost all of the gold surface ($\theta > 0.9$) becomes covered with thiol during the first few minutes. However, the formation of a nearly passivating monolayer ($\theta \rightarrow 1$) requires a longer time period. None of our experimental curves belongs to zone 4, where $R_d >> 10^{-5}$ cm. This observation agrees with the SECM results of $R_d < 5 \times 10^{-5}$ cm for any exposure time.

SECM Approach Curves

Figure 4 shows the current–distance curves for a 3.5-μm-radius C tip UME approaching a gold substrate that

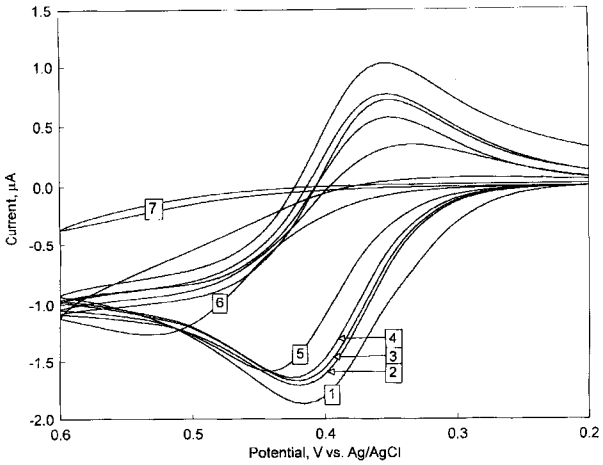

Fig. 3. Cyclic voltammograms of 2×10^{-3} M $FcTMAPF_6$ at a 0.5-mm-radius gold electrode pre-exposed to a 5 mM solution of hexadecyl mercaptan. $v = 10$ mV/s. t_e = (1) 0, (2) 1, (3) 5, (4) 10, (5) 20, (6) 40, and (7) 50 min. The aqueous solution also contained 0.2 M LiCl.

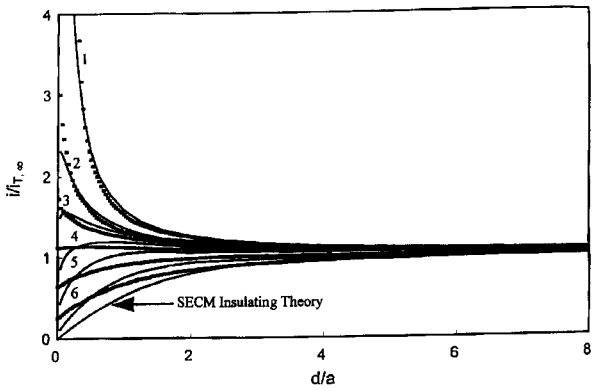

Fig. 4. Current–distance curves for a 3.5-μm-radius C tip UME approaching the gold substrate partially passivated by hexadecyl mercaptan. The tip was biased at +0.45 vs. Ag/AgCl (3 M KCl) in an aqueous solution containing 2×10^{-3} M $FcTMAPF_6$ and 0.2 M LiCl. The tip scan rate was 0.05 μm/s. t_e = (1) 0, (2) 1, (3) 10, (4) 15, (5) 20, and (6) 55 min. Solid lines represent SECM theory (eq 11) with k_{eff} = (1) ∞ (conductive substrate), (2) 2.75, (3) 1.65, (4) 0.88, (5) 0.42, and (6) 0.08 cm/s. The corresponding $(1 - \theta)/R_d$ values obtained from eq 6 are (1) ∞, (2) 6750, (3) 4050, (4) 2160, (5) 1031, and (6) 209 cm^{-1}.

was pre-exposed to a 5 mM solution of hexadecyl mercaptan. The approach curves in Fig. 4 fit the SECM theory, assuming finite heterogeneous kinetics at the substrate (solid curves calculated from eq 11). The values of the normalized effective rate constant, ak_{eff}/D = 2.75, 1.65, 0.88, 0.42, and 0.08, were calculated for exposure times, t_e = 1, 10, 15, 20, and 55 min. However, all experimental approach curves were obtained with the substrate potential sufficiently negative to reduce the oxidized form of the mediator at the defect sites at a diffusion-controlled rate. Thus, the apparent kinetic limitations are due to partial blocking of the substrate surface and can be determined according to eq 6. The $(1 - \theta)/R_d$ values obtained from eq 6 are 6750, 4050, 2160, 1031, and 209 cm^{-1} for the above exposures. These values are in agreement with the discussed semiquantitative CV results.

Chronoamperometry

Typical chronoamperograms of $FcTMAPF_6$ at a 0.5-mm-radius gold electrode are shown in Fig. 5. The i vs. $t^{-1/2}$ (t in s) curves were obtained with a 1-mm-diameter Au electrode pre-exposed to a 5 mM solution of hexadecyl mercaptan for 0, 1, 5, 10, 20, and 40 min. To improve clarity of the presentation, only i–$t^{-1/2}$ curves for 1, 20, and 40 min are shown in Fig. 5. The first chronoamperogram obtained at a bare Au electrode fits the Cottrell equation (solid line) quite well. The slope of that straight line yields the value $nFc^{\circ}A\sqrt{D/\pi} = 2.799 \times 10^{-6}$ $s^{-1/2}$ which was used to fit other chronoamperograms to eq 14. The shape of the i vs. t curve is largely determined by the value of a single adjustable parameter, $(1 - \theta)/R_d$, which accounts for both coverage effect and defect radius. The calculated $(1 - \theta)/R_d$ values for the experimental curves decreased monotonically as the thiol exposure time increased. The values of $(1 - \theta)/R_d$ = 17142, 7145, 7142, 5000, and 643 obtained for t_e = 1, 5, 10, 20, and 40 min, respectively, show the same trend found in our SECM and CV data. The lack of close quantitative agreement between chronoamperometric and SECM results is probably due to different approximations used in derivations of the above theoretical expressions, as well as the random character of the polished electrode surface which greatly contributes to the irreproducibility of the adsorption experiments.

The decrease in $(1 - \theta)/R_d$ can either point to an increasing surface coverage or increasing average defect radius. To separate these two effects, we obtained charging current transients by application of potential steps from 0 to 0.55 V vs. Ag/AgCl to a gold electrode after it was pre-exposed to the thiol solution (Fig. 6). The capacitance of the bare Au electrode in a 0.2 M LiCl solution was 33.8 μF/cm^2, and after 50 min of exposure to the thiol solution, the capacitance reached a constant value of about 5 μF/cm^2. Both of these values are in agreement with those previously reported.[24] The θ values for smaller t_e can be calculated according to the formula:[25]

$$\theta = \frac{C - C_o}{C_{mon} - C_o} \qquad (22)$$

where C_o = 33.8 μF/cm^2 is the capacitance of a bare gold

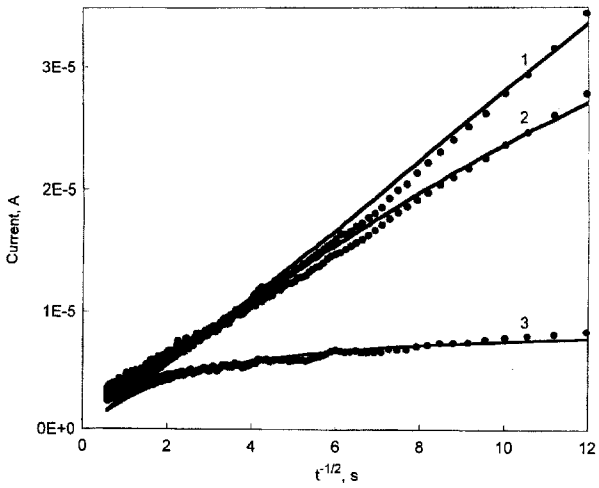

Fig. 5. Chronoamperograms of ferrocenylmethyltrimethylammonium hexafluorophosphate at a 0.5-mm-radius gold electrode pre-exposed to a 5×10^{-3} M solution of hexadecyl mercaptan. The electrode potential was stepped from 0 to 0.55 V vs. Ag/AgCl (3 M KCl). t_e = (1) 0, (2) 20, and (3) 40 min. The theoretical curves (solid lines) were computed from eq 14 with $n = 1$, $c^\circ = 2 \times 10^{-3}$ M, $D = 5 \times 10^{-6}$ cm^2/s, and $A = 0.00785$ cm^2. The corresponding $(1 - \theta)/R_d$ values obtained from eq 14 are (1) ∞ (Cottrell equation), (2) 17142, (3) 7145, (4) 7142, (5) 5000, and (6) 643 cm^{-1}.

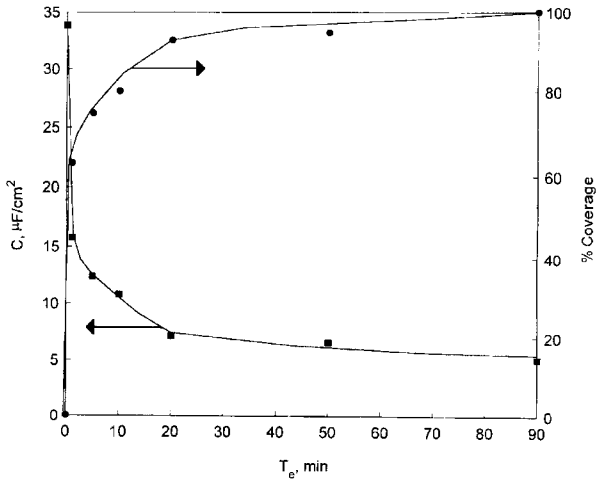

Fig. 6. Capacitance (left scale) and corresponding surface coverage (right scale) values for a 1-mm-diameter gold electrode pre-exposed to a 5 mM solution of hexadecyl mercaptan. t_e = (1) 0, (2) 1, (3) 5, (4) 10, (5) 20, (6) 50, and (7) 90 min. The capacitance was measured from potentiostatic transients in 0.2 M LiCl solution. The potential was stepped from 0 to 0.55 V vs. Ag/AgCl (3 M KCl). Surface coverage was calculated from eq 22.

electrode and $C_{mon} = 5$ μF/cm^2 is the capacitance of the complete monolayer. The calculated θ increases monotonically with t_e, which probably causes the decrease in $(1 - \theta)/R_d$ found in our CV and SECM measurements. The change in capacitance with t_e after 10–20 min is very small, indicating that the surface is nearly completely covered with thiol. The precision of these measurements is not high enough to extract θ from these results. However, the surface coverage after 1 min of exposure yields a more reliable value of $\theta \approx 0.6$. From this value and $(1 - \theta)/R_d = 17142$ cm^{-1}, one finds $R_d \approx 2 \times 10^{-5}$ cm. In contrast, a much smaller $R_d = 3$ nm was found previously for a complete thiol monolayer on gold.[26] Combining this value with $(1 - \theta)/R_d = 209$ cm^{-1} obtained from the SECM approach curve after 55 min of exposure, one finds $1 - \theta = 6.3 \times 10^{-5}$ and the density of defects of about 2×10^8 cm^{-2}. Apparently, the rearrangement of a SAM takes a much longer time than 55 min and eventually leads to a film with low defect density,[7] but the later stages of this process are difficult to monitor electrochemically.

CONCLUSIONS

The adsorption of hexadecyl mercaptan from millimolar solutions onto a gold surface is rapid (probably diffusion-controlled), with > 90% of the Au substrate being covered in a few minutes. At this stage, the film appears to be macroscopically uniform, and the defects are smaller than 0.5 μm in radius. The subsequent rearrangement (annealing) of the thiol layer is much slower and results in the formation of a more compact film. The results obtained with different electrochemical techniques, i.e., SECM, chronoamperometry, and cyclic voltammetry, showed both a slow increase in the surface coverage and a decrease of the average defect radius taking place at this stage. After 50–60 min of exposure of the Au surface to thiol, the surface coverage approaches unity (θ > 99.9 %), making the electric current through the defects too low for electrochemical measurements. However, a considerable density of nanometer-sized defects on the order of 10^8 cm^{-2} still remains in the film. The formation of lower-defect films probably takes many hours.

While in this study we dealt mainly with the high coverage of Au surfaces by thiol, it would also be useful to investigate the initial stages of SAM formation (i.e., θ < 50%) with the SECM. Mapping surface reactivity with submicrometer-scale resolution should allow observation of the monolayer growth pattern, e.g., islands vs. expanding compact layer.

Acknowledgments. The support of this research by grants from the Robert A. Welch Foundation and the National Science Foundation (CHE-9508525, A.J.B.) is gratefully acknowledged. M.V.M. also acknowledges a grant from PSC-CUNY.

REFERENCES AND NOTES

(1) Nuzzo, R.G.; Fusco, F.A.; Allara, D.L. *J. Am. Chem. Soc.* **1987**, *109*, 2358–2368.

(2) Porter, M.D.; Bright, T.B.; Allara D.L.; Chidsey, C.E. *J. Am. Chem. Soc.* **1987**, *109*, 3559–3568.

(3) Chidsey, C.E.; Bertozzi, C.R.; Putvinski, T.M.; Mujasce, A.M. *J. Am. Chem. Soc.* **1990**, *112*, 4301–4306.

(4) Stranick, S.J.; Parikh, A.N.; Tao, Y.-T.; Allara, D.L.; Weiss, P.S. *J. Phys. Chem.* **1994**, *98*, 7636–7646.

(5) Sagiv, J. *J. Am. Chem. Soc.* **1980**, *102*, 92-98.

(6) Zhao, X.-M.; Wilbur, J.L.; Whitesides, G.M. *Langmuir* **1996**, *12*, 3257–3264.

(7) Finklea, H.O. In Electroanalytical Chemistry; Bard, A.J.; Rubinstein, I., Eds.; Marcel Dekker: New York, 1996; Vol. 19, pp 109–335.

(8) (a) Miller C.; Gratzel, M. *J. Phys. Chem.* **1991**, *95*, 5225–5233. (b) Finklea, H.O.; Snider, D.A.; Fedyk, J.; Sabatani, E.; Gafni, Y.; Rubinstein, I. *Langmuir* **1993**, *9*, 3660–3667.

(9) (a) Kumar, A.; Abbott, N.L.; Whitesides, G.M. *Acc. Chem. Res.* **1995**, *28*, 219–226. (b) Noy, A.; Frisbie, C.D.; Rozsnyai, L.F.; Wrighton, M.S.; Lieber, C.M. *J. Am. Chem. Soc.* **1995**, *117*, 7943–7951.

(10) Bilewicz, R.; Majda, M. *J. Am. Chem. Soc.* **1991**, *113*, 5464–5466.

(11) Bard, A.J.; Mirkin, M.V.; Unwin, P.R.; Wipf, D.O. *J. Phys. Chem.* **1992**, *96*, 1861–1868.

(12) Landsberg, R.; Thiele, R. *Electrochim. Acta* **1966**, *11*, 1243–1259.

(13) (a) Zwanzig, R. *Proc. Natl. Acad. Sci. U.S.A.* **1990**, *87*, 5856–5857. (b) Zwanzig R.; Szabo, A. *Biophys. J.* **1991**, *60*, 671–678.

(14) Szabo, A.; Zwanzig, R. *J. Electroanal. Chem.* **1991**, *314*, 307–311.

(15) Amatore, C.; Savéant, J.M.; Tessier, D. *J. Electroanal. Chem.* **1983**, *147*, 39–51.

(16) Oldham, K.B.; Zoski, C.G. *J. Electroanal. Chem.* **1988**, *256*, 11–19.

(17) Wei, C.; Bard A.J.; Mirkin, M.V. *J. Phys. Chem.* **1995**, *99*, 16033–16042.

(18) Mirkin, M.V.; Fan F.-R.F.; Bard, A.J. *J. Electroanal. Chem.* **1992**, *328*, 47–62.

(19) Smythe, W.R.; *J. Appl. Phys.* **1953**, *24*, 70–78.

(20) Berg, H.C.; Purcell, E.M. *Biophys. J.*, **1977**, *20*, 193–239.

(21) Bard, A.J.; Fan, F.-R.F.; Kwak, J.; Lev, O. *Anal. Chem.* **1989**, *61*, 1794–1799.

(22) Wipf, D.O.; Bard, A.J. *J. Electroanal. Chem.* **1991**, *138*, 469–474.

(23) (a) Gueshi, T.; Tokuda, K.; Matsuda, H. *J. Electroanal. Chem.* **1978**, *89*, 247–260; (b) Gueshi, T.; Tokuda, K.; Matsuda, H. *J. Electroanal. Chem.* **1979**, *101*, 29–38; (c) Tokuda, K.; Gueshi, T.; Matsuda, H. *J. Electroanal. Chem.* **1979**, *102*, 41–48.

(24) Smalley, J.F.; Feldberg, S.W.; Chidsey, C.E.D.; Linford, M.R.; Newton, M.D.; Liu, Y.-P. *J. Phys. Chem.* **1995**, *99*, 13141–13149.

(25) Yamane, M.; Kakiuchi, T.; Osakai, T.; Senda M. *Rev. Polarogr.* (Kyoto) **1983**, *29*, 102.

(26) Sun, L.; Crooks, R.M. *J. Electrochem. Soc.* **1991**, *138*, L23–L25.